Gama et al., https://doi.org/10.1083/jcb.201610108

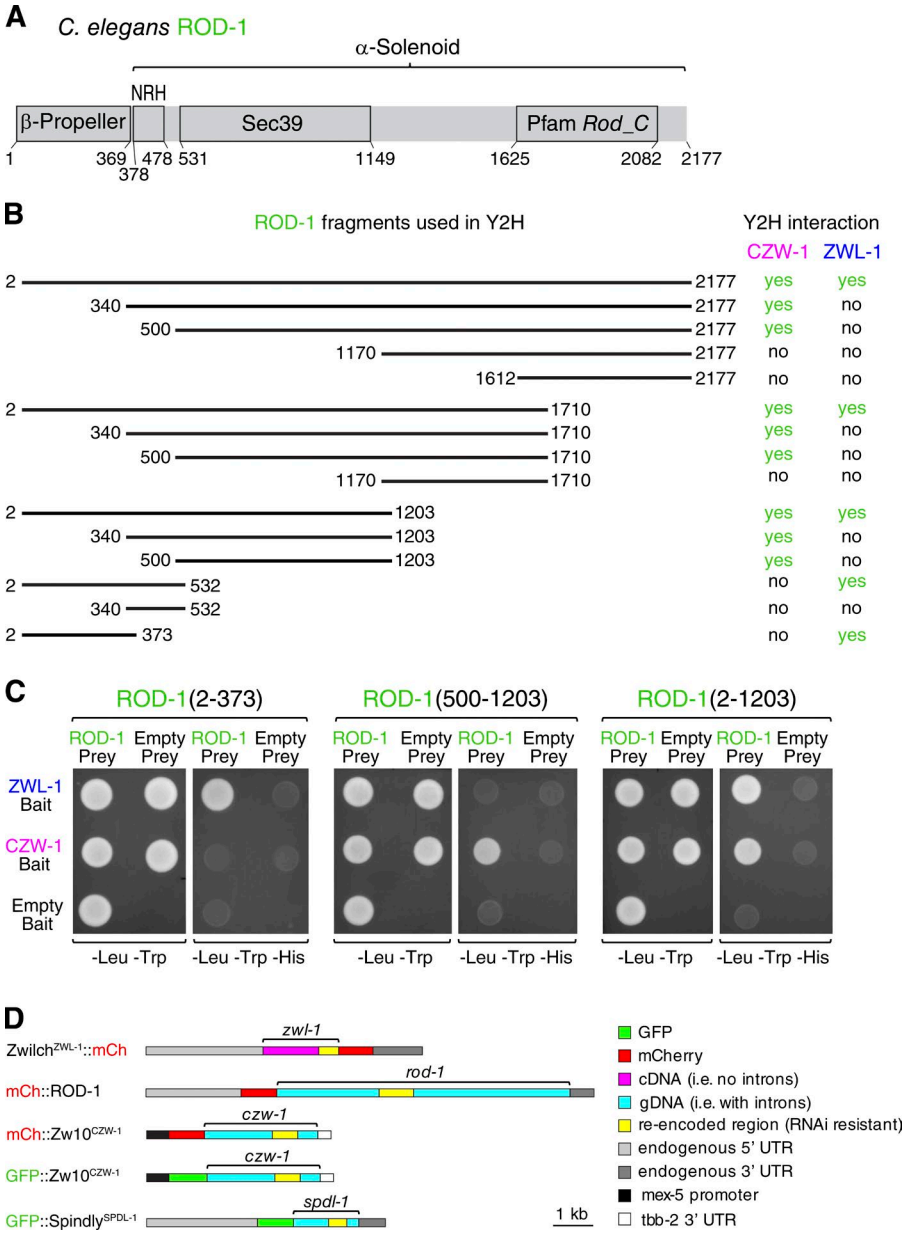

Figure S1. **Identification of ROD-1 fragments that interact with Zwilch^{ZWL-1} and Zw10^{CZW-1}.** (A) Cartoon showing the domain organization of *C. elegans* ROD-1. The N-terminal β-propeller is followed by the NAG–ROD homology (NRH) domain. The Sec39 domain is followed by another 1,000 residues containing a conserved C-terminal region annotated in the Pfam database (ROD_C; PF10493). After the β-propeller, ROD-1 is predicted to adopt an α-solenoid structure of stacked helices. (B) List of the 15 ROD-1 fragments tested in yeast two-hybrid (Y2H) experiments against full-length Zwilch^{ZWL-1} and Zw10^{CZW-1}. The shortest Zwilch^{ZWL-1}-binding fragment corresponds to the β-propeller domain, and the shortest Zw10^{CZW-1}-binding fragment corresponds to the Sec39 domain. We also tested all ROD-1 fragments against each other but failed to detect any interactions, nor did we detect an interaction between Zwilch^{ZWL-1} and Zw10^{CZW-1}. (C) Results of the yeast two-hybrid experiment with the minimal ROD-1 fragments capable of interacting with Zwilch^{ZWL-1} only (ROD-1$^{2–373}$), Zw10^{CZW-1} only (ROD-1$^{500–1,203}$), or with both Zwilch^{ZWL-1} and Zw10^{CZW-1} (ROD-1$^{2–1,203}$). Cells containing bait and prey plasmids grow on -Leu/-Trp plates, whereas -Leu/-Trp/-His plates select for the interaction between bait and prey. (D) Cartoons of RNAi-resistant transgenes used to generate *C. elegans* strains by Mos1-mediated single copy insertion.

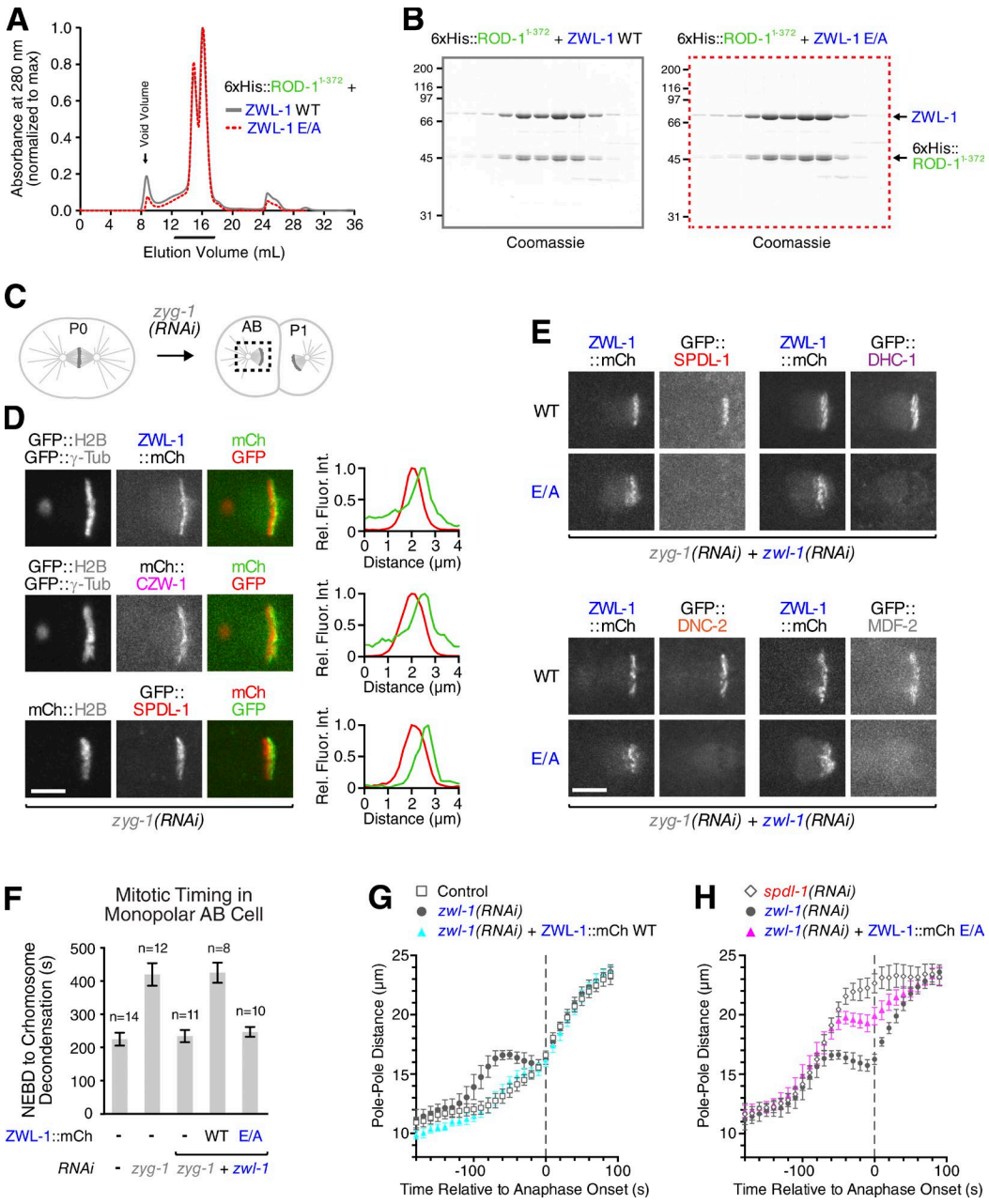

Figure S2. **The Zwilch^{ZWL-1} E433A/E437A mutant fails to recruit dynein, dynactin, and Mad2^{MDF-2} to kinetochores and causes defects in kinetochore–microtubule attachment and SAC signaling.** (A and B) Elution profiles and Coomassie-stained protein gels of size-exclusion chromatography experiments on ROD-1$^{1–372}$ in complex with either wild-type Zwilch^{ZWL-1} or the E/A mutant. The fraction range shown in the protein gels is demarcated by the bar below the elution profile. Molecular mass is indicated in kilodaltons. (C) Cartoon illustrating the experimental strategy to generate monopolar spindles in the second embryonic division. ZYG-1 is a kinase required for centriole duplication. In *zyg-1(RNAi)* embryos, the first division is normal because two intact centrioles are contributed by sperm that is not affected by RNAi. Centrioles are unable to duplicate, resulting in a monopolar spindle in the subsequent division. (D) Still images from time-lapse sequences of monopolar AB cell divisions in embryos coexpressing Zwilch^{ZWL-1}::mCherry, mCherry::Zw10^{CZW-1}, or GFP::Spindly^{SPDL-1} with markers for spindle poles and chromosomes. The single spindle pole is always positioned on the left. Fluorescence line scans show asymmetric enrichment of RZZ subunits and GFP::Spindly^{SPDL-1} at microtubule-unattached kinetochores located on the chromosomal side facing away from the single pole. (E) Stills from time-lapse sequences as described in D in embryos coexpressing Zwilch^{ZWL-1}::mCherry with GFP::Spindly^{SPDL-1}, GFP::dynein heavy chain^{DHC-1}, GFP::dynactin p50^{DNC-2}, or GFP::Mad2^{MDF-2}. The Zwilch^{ZWL-1}::mCherry E/A mutant fails to recruit any of these components to unattached kinetochores. Bars, 5 µm. (F) Mean interval between nuclear envelope breakdown and chromosome decondensation in the AB cell of embryos expressing GFP::histone H2B. Monopolar spindle formation after ZYG-1 depletion results in a SAC-dependent mitotic delay. Wild-type (WT) Zwilch^{ZWL-1}::mCherry, but not the E/A mutant, rescues the delay. This demonstrates that the Zwilch^{ZWL-1}::mCherry E/A mutant is defective in SAC signaling. The number (n) of embryos scored is indicated. (G) Plot of spindle pole separation kinetics in one-cell embryos expressing GFP::γ-tubulin, which serves as a readout for kinetochore–microtubule attachment formation. Transgene-encoded Zwilch^{ZWL-1}::mCherry rescues the premature pole separation caused by the lack of kinetochore dynein in embryos depleted of endogenous Zwilch^{ZWL-1}. Images were acquired at 10-s intervals, and sequences were time-aligned relative to the onset of sister chromatid separation (Anaphase Onset). Pole–pole distances in the time-aligned sequences were measured, averaged for the indicated number (n) of embryos, and plotted against time. (H) Plot of spindle pole separation kinetics as described in G, showing that premature pole separation in the Zwilch^{ZWL-1} E/A mutant is significantly more severe than in Zwilch^{ZWL-1} depletions, as predicted by the absence of kinetochore dynein. Error bars represent the SEM with a 95% confidence interval.

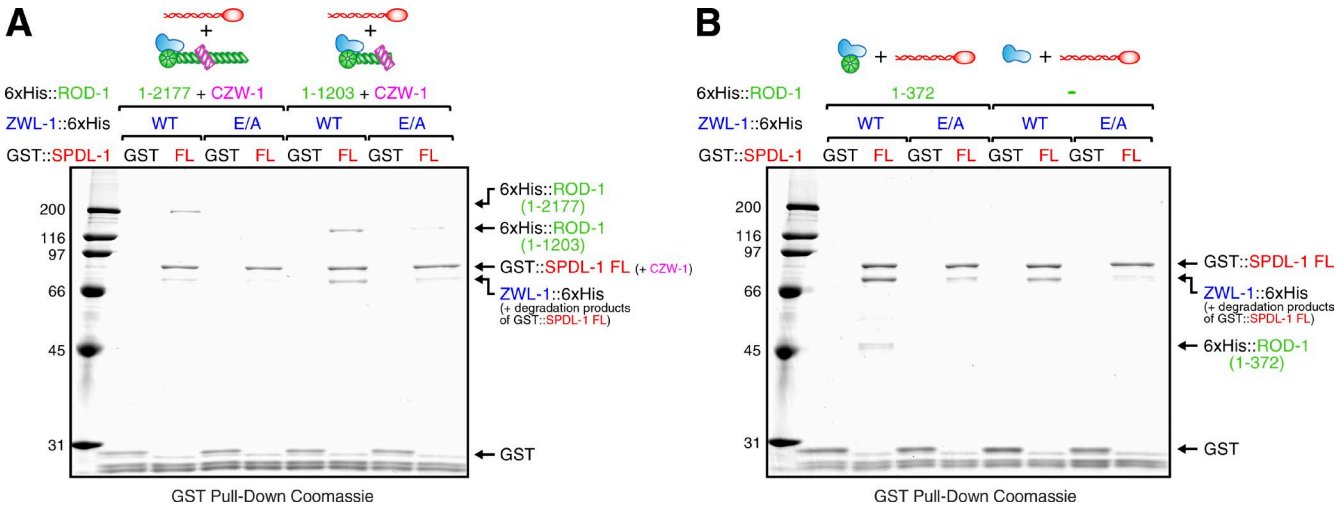

Figure S3. **Spindly^{SPDL-1} binding to RZZ depends on Zwilch^{ZWL-1} residues E433/E437.** (A and B) Coomassie-stained protein gels of the GST::Spindly^{SPDL-1} pull-downs from insect cell lysates containing different versions of RZZ, obtained by baculovirus-driven expression. The gels correspond to the immunoblots shown in Fig. 3 (C and D). Note that Zwilch^{ZWL-1} migrates at the same size as degradation products of GST::Spindly^{SPDL-1} (see Fig. 3 B) and that Zw10^{CZW-1} migrates at the same size as GST::Spindly^{SPDL-1}. Molecular mass is indicated in kilodaltons. FL, full-length; WT, wild type.

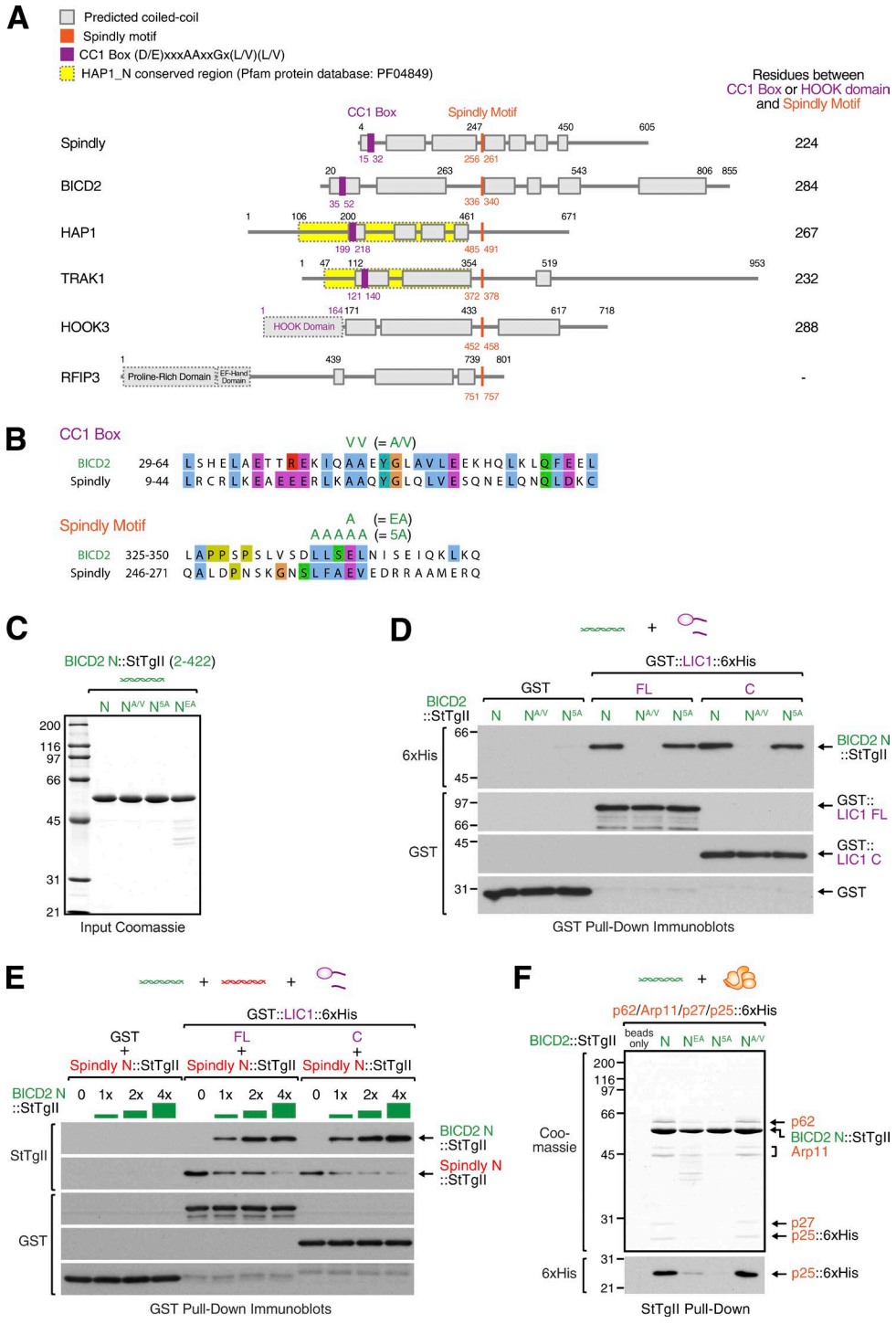

Figure S4. **Spindly and the dynein adaptor BICD2 use a similar mechanism to engage with dynein and dynactin.** (A) Cartoons showing the domain architecture of Spindly, BICD2, and additional dynein adaptors that contain a conserved region in their first coiled-coil segment (CC1 box) and/or a motif with homology to the Spindly motif required for dynein–dynactin recruitment to kinetochores. In Spindly, BICD2, HAP1, TRAK1, and Hook3, the CC1 box/Hook domain is separated from the Spindly-like motif by a coiled-coil region with a mean size of 260 residues. In BICD2, the coiled-coil binds along the Arp1 filament of dynactin in an orientation that places BICD2's N-terminal CC1 box at the barbed end and BICD2's Spindly-like motif near the pointed end (Urnavicius et al., 2015). (B) The CC1 box and Spindly-like motif of BICD2 with the mutations used in subsequent panels are indicated. (C) Coomassie-stained protein gels of purified wild-type and mutant BICD2$^{2–422}$ fused to Strep-tag II (StTgII). (D) Immunoblots of GST pull-downs using the BICD2 fragments in C and the GST::LIC1 proteins shown in Fig. 5 C, demonstrating that the N-terminal coiled-coil region of BICD2 binds the C-terminal region of LIC1. The interaction is abolished in the BICD2 A/V mutant, but not in the 5A mutant. Protein fractions bound to beads were detected on blots with Strep-Tactin. The same membrane was then reprobed with anti-GST antibody. (E) Immunoblots of GST pull-downs as in D showing that BICD2$^{2–422}$ and Spindly$^{2–359}$ compete for binding to the C-terminal region of LIC1. Increasing amounts of BICD2$^{2–422}$ were added to a constant amount of Spindly$^{2–359}$ and full-length GST::LIC1 or GST::LIC1$^{388–523}$. (F) Coomassie-stained gel and immunoblot of Strep-tag II pull-downs using the purified dynactin pointed-end complex (see Fig. 5 G) and the BICD2 fragments in C. The interaction between BICD2's N-terminal coiled-coil and dynactin pointed-end complex is diminished by point mutations in BICD2's Spindly-like motif (EA and 5A) but not by the A/V mutant. Molecular mass is indicated in kilodaltons.

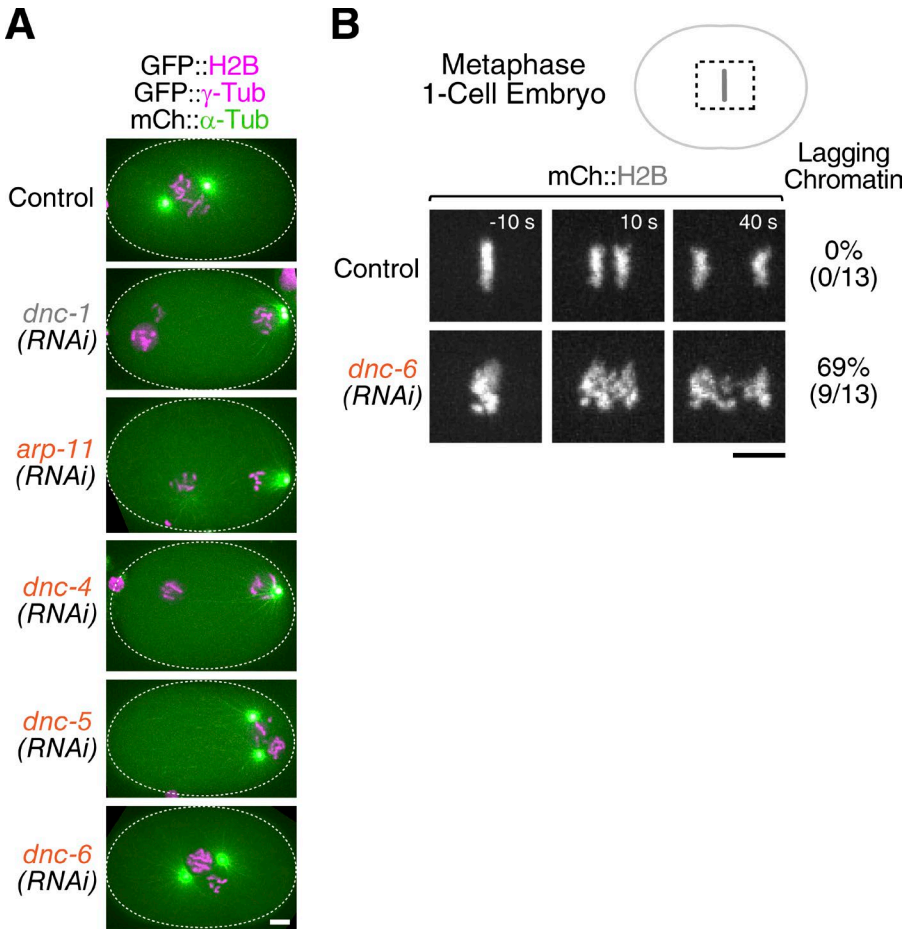

Figure S5. **Phenotype of dynactin pointed-end subunit depletions in the *C. elegans* one-cell embryo.** (A) Stills from time-lapse sequences in embryos coexpressing mCherry::α-tubulin, GFP::γ-tubulin, and GFP::histone H2B. The time point shown is nuclear envelope breakdown. Depletion of Arp-11 and p62^{DNC-4} causes defects that are indistinguishable from those of p150^{DNC-1} depletions and reflect the "dynactin-null" phenotype. In contrast, depletion of p25^{DNC-5} and p27^{DNC-6} causes less severe defects, indicating that they are not required for all of dynactin's functions. Although p25^{DNC-5}-depleted embryos still exhibit mild defects during pronuclear migration, p27^{DNC-6} depletion results in a specific defect in chromosome segregation without affecting the dynein–dynactin-dependent positioning of centrosomes and nuclei. (B) Selected frames from time-lapse sequences in embryos expressing mCherry::histone H2B, showing the chromosome segregation defect after p27^{DNC-6} depletion. Time is relative to anaphase onset. Bars, 5 µm.

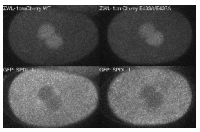

Video 1. **The Zwilch^{ZWL-1} E433A/E437A mutant displaces Spindly^{SPDL-1} from kinetochores.** The anterior of the embryo is to the left, and the posterior of the embryo is to the right. Time lapse is 10 s; playback speed is six frames per second.

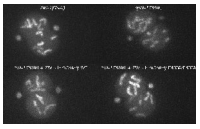

Video 2. **The Zwilch^{ZWL-1} E433A/E437A mutant causes chromosome segregation defects that resemble those of Spindly^{SPDL-1} depletions.** Chromosomes and spindle poles are labeled with GFP::histone H2B and GFP::γ-tubulin, respectively. The anterior of the embryo is to the left, and the posterior of the embryo is to the right. Time lapse is 10 s; playback speed is six frames per second.

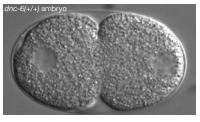

Video 3. **First embryonic divisions in the absence of p27^{DNC-6} imaged using differential interference contrast, showing normal pronuclear migration and spindle positioning but defective chromosome segregation leading to multinucleate cells (indicated by arrows).** The anterior of the embryo is to the left, and the posterior of the embryo is to the right. Time lapse is 5 s; playback speed is 12 frames per second.

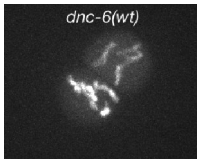

Video 4. **First embryonic division in the absence of p27^{DNC-6} with mCherry-labeled histone H2B to visualize chromosome segregation.** The anterior of the embryo is to the left, and the posterior of the embryo is to the right. Time-lapse is 10 s; playback speed is six frames per second.

Table S1 is a separate Excel file and is a list of worm strains used in this study.

Table S2 is a separate Excel file and is a list of oligonucleotides used in this study for dsRNA production.

Reference

Urnavicius, L., K. Zhang, A.G. Diamant, C. Motz, M.A. Schlager, M. Yu, N.A. Patel, C.V. Robinson, and A.P. Carter. 2015. The structure of the dynactin complex and its interaction with dynein. *Science.* 347:1441–1446. http://dx.doi.org/10.1126/science.aaa4080